

Looking for (Genomic) Needles in a Haystack: Sparsity-Driven Search for Identifying Correlated Genetic Mutations in Cancer

Ritvik Prabhu*, Emil Vatai[¶], Bernard Moussad^{*¶}, Emmanuel Jeannot[§],
Ramu Anandkrishnan[‡], Wu-chun Feng*, Mohamed Wahib[†]

^{*}*Department of Computer Science, Virginia Tech, Blacksburg, USA*

[‡]*Biomedical Sciences, Edward Via College of Osteopathic Medicine, Blacksburg, USA*

Email: {ritvikp,bernardm,ramu,wfeng}@vt.edu

[§]*Inria, Univ. Bordeaux, LaBRI, Talence, France*

Email: emmanuel.jeannot@inria.fr

[†]*RIKEN Center for Computational Science, Kobe, Japan*

Email: {emil.vatai,mohamed.attia}@riken.jp

Abstract—Cancer typically arises not from a single genetic mutation (i.e., hit) but from multi-hit combinations that accumulate within cells. However, enumerating multi-hit combinations becomes exponentially more expensive computationally as the number of candidate hit gene combinations grow, i.e. $C_h^{20,000}$, where 20,000 is the number of genes in the human genome and h is the number of hits. To address this challenge, we present an algorithmic framework, called Pruned Depth-First Search (P-DFS) that leverages the high sparsity in tumor mutation data to prune large portions of the search space. Specifically, P-DFS (the main contribution of this paper) - a pruning technique that exploits sparsity to drastically reduce the otherwise exponential h -hit search space for candidate combinations used by Weighted Set Cover - which is grounded in a *depth-first search backtracking* technique, prunes infeasible gene subsets early, while a standard greedy *weighted set cover* (WSC) formulation systematically scores and selects the most discriminative combinations.

By intertwining these ideas with optimized bitwise operations and a scalable distributed algorithm on high-performance computing clusters, our algorithm can achieve $\approx 90 - 98\%$ reduction in visited combinations for 4-hits, and roughly a $183 \times$ speedup over the exhaustive set cover approach (which is algorithmically NP-complete) measured on 147,456 ranks. In doing so, our method can feasibly handle four-hit and even higher-order gene hits, achieving both speed and resource efficiency.

I. INTRODUCTION

Genetic mutations occur routinely in our cells, yet most of these mutations are benign. Occasionally, however, a specific subset of mutations arises that can pave the way for cancer development. Cancer itself is not a single disease, rather, it is a diverse group of disorders defined by unchecked cell growth [1]. Despite decades of effort, it remains the second leading cause of death worldwide, projected to claim around 618,120 lives in the United States alone in 2025 [2]. The crux of the challenge lies in the fact that cancer typically does not emerge from a single genetic mutation (“hit”) but rather from

precise, multi-hit combinations of a small number (typically between 2–9 hits) of genetic alterations [3].

Understanding these multi-hit patterns has profound implications. First, it illustrates how cancer starts and progresses, providing insight into the biological mechanisms behind tumor formation. Second, identifying the exact sets of mutations responsible for a given case of cancer can guide the design of more targeted combination therapies [4], [5]. Nevertheless, pinpointing these critical mutation sets is akin to searching for needles in a genomic haystack. With roughly 20,000 genes in the human genome [6], even two-hit combinations yield on the order of 2×10^8 possibilities, while four-hit and five-hit combinations balloon into the range of 10^{15} to 10^{19} , respectively. Exhaustively exploring all such combinations quickly overwhelms traditional computational approaches; recent estimates suggest that identifying all four-hit combinations would require over 500 years on a single CPU [7].

To tackle this challenge, multi-hit combination analysis has emerged as a prominent strategy. At its core, this approach aims to pinpoint which specific combinations of genetic mutations are most relevant to carcinogenesis, i.e. the process by which normal cells transform into cancer cells. One leading paradigm views the task as a weighted set cover (WSC) problem, an NP-complete problem, where each candidate mutation set “covers” the tumor samples carrying that set and ideally excludes normal samples [8]. Although WSC can be highly accurate, all possible gene combinations must be exhaustively enumerated, an endeavor that grows exponentially with each additional “hit.” Even powerful high-performance computing (HPC) systems struggle to search beyond three-hit or four-hit mutation sets without encountering prohibitively large runtimes or system limitations like I/O bottlenecks, memory constraints, and communication overhead [7].

To cope with the exponential explosion of the search space, researchers have explored heuristics that avoid enumerating

[¶] Emil Vatai and Bernard Moussad contributed equally to this work.

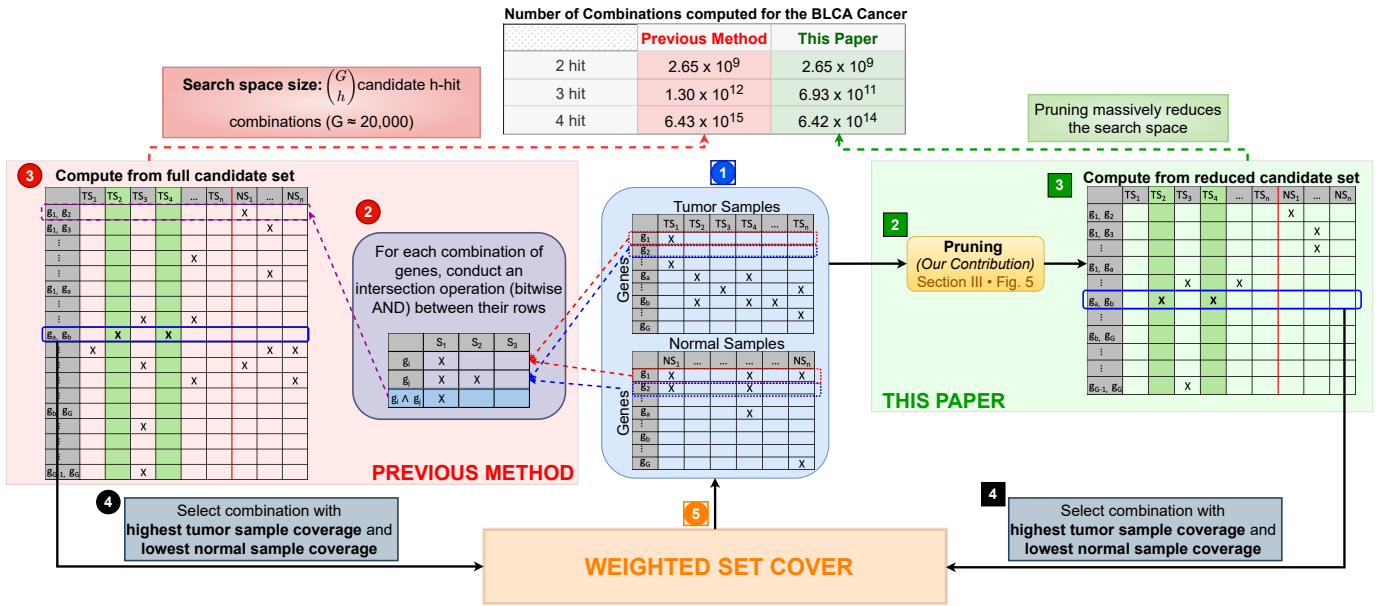


Fig. 1: Overview of workflow. ① **Input:** tumor and normal mutation matrices, represented as per-gene bitsets over samples. ②–③ **Previous method (exhaustive enumeration):** for every h -hit gene combination, the prior pipeline performs a bitwise AND across the corresponding gene rows (②) and computes over the full candidate table (③), which quickly becomes intractable as h grows. ②–③ **This paper (prune-then-evaluate):** our main contribution is P-DFS, a sparsity-driven pruned depth-first search that *massively prunes* the h -hit search space (②) before scoring (see §III and Fig. 5). This produces a substantially smaller candidate table to evaluate (③), yielding significant compute-time savings by avoiding bitwise-AND intersections for the vast majority of combinations. ④ and ④ **Selection step (common to both):** choose the candidate combination with highest tumor coverage and lowest normal coverage, and pass it into the weighted set cover procedure ⑤. The table at the top summarizes the resulting reduction in combinations explored, which becomes more pronounced as the number of hits h increases.

the entire combination space. One such approach, BiGPICC, quickly identifies higher-order hits by leveraging a graph-based method. However, BiGPICC omits large swaths of the combination space in the name of speed, which can degrade classification accuracy [9]. In practice, then, the cancer-genomics community faces a trade-off: comprehensive methods that handle only a few hits versus heuristic-based approaches that find more hits but risk missing the precise “needles” in the genomic haystack.

In this paper, we introduce a novel HPC-driven framework to push the boundary of multi-hit analyses. We build upon the rigor of WSC-based methodology but overcome its typical limitations through the utilization of advanced supercomputing resources and optimizations that capitalize on the sparsity inherent to carcinogenesis data. By doing so, our approach navigates the massive search space that was previously considered intractable. Specifically, we introduce a new algorithm, *pruned depth-first search* (P-DFS) for traversing the search space of multi-hit combinations—our main contribution, which reduces the otherwise exhaustive candidate search space that dominates WSC-based pipelines (Fig. 1). In particular, we leverage the high sparsity in gene mutations to do a distributed depth-first search with backtracking to prune the combinatorial search space, thereby shrinking the candidate set before applying the *standard greedy* WSC selection step, thus dramatically improving the efficiency.

Through this effort, we seek not only to advance our understanding of the genetics underlying cancer but also to provide a practical path toward precisely tailored combination therapies that could improve outcomes for patients worldwide.

The remainder of the paper proceeds as follows. In §II, we review background and related work on multi-hit modeling and search formulations. §III presents our pruned depth-first search (P-DFS) method, including sparsity-aware preprocessing, the core pruning algorithm, and topology-aware work distribution with hierarchical collectives. §IV reports the results on the Fugaku supercomputer, including datasets, pruning efficiency, accuracy on held-out data, load balancing with work stealing, and strong scaling. §V provides a summary of our findings.

II. BACKGROUND AND RELATED WORK

A. Historical Foundations of the Multi-Hit Concept

A seminal moment in understanding cancer’s genetic basis came from Alfred Knudson’s 1971 “two-hit hypothesis,” which suggested that certain cancers, specifically retinoblastoma, emerge only after mutations have occurred in both copies of a tumor suppressor gene [10]. While Knudson focused on a rare pediatric tumor, his ideas gave rise to a wave of research showing that various solid tumors (e.g., breast, colon, and colorectal cancers) likely require multiple genetic “hits” to shift from normal cellular regulation to malignant growth [11]–[13].

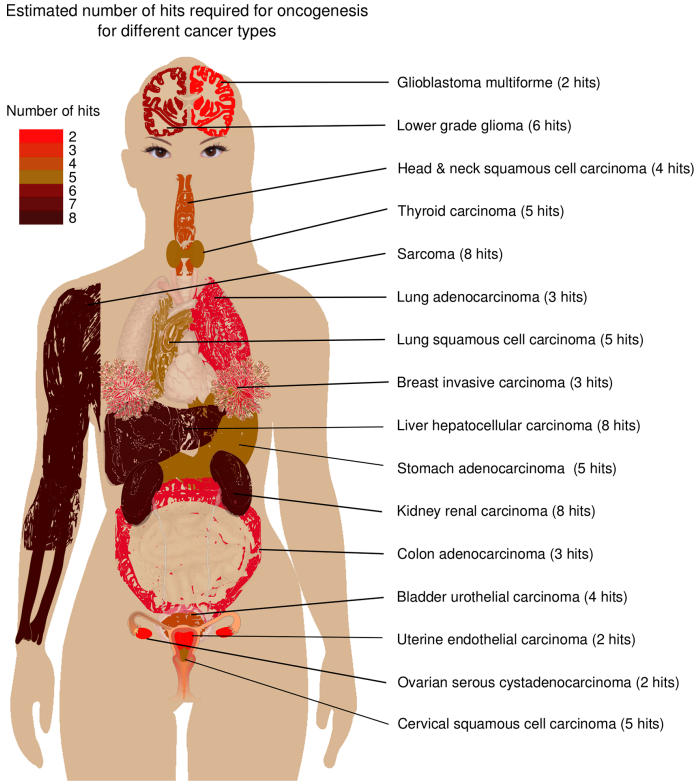


Fig. 2: Visualization of estimated hit numbers for each cancer type from [3]. Derived from the public domain image by M. Haggstrom (2014) [18].

Over the following decades, scientists increasingly recognized that no single “magic number” of hits applies universally across all tumor types. This led to a deeper statistical and mathematical modeling of carcinogenesis. Early modeling efforts often assumed relatively simple, uniform mutation rates across genes [14]–[17], but they could not account for the variability in how fast or slow different genes accumulate alterations. Building upon these limitations, Anandakrishnan et al. introduced a more data-driven model that focuses on the observed distribution of somatic mutations rather than on any single pre-specified rate [3]. They established that many cancers seem to arise from combinations of between 2 and 9 hits, depending on tumor type.

As shown in Fig. 2, the number of hits required can vary, reinforcing the idea that cancer is not a single entity but rather a multitude of genetic scenarios each leading to a common endpoint of tumor formation. This insight highlights the importance of developing comprehensive computational tools capable of sifting through a large and heterogeneous genomic search space.

B. Approaches for Identifying Multi-Hit Combinations

From a computer science perspective, the multi-hit problem can be formulated as follows. Given a binary mutation matrix $X \in \{0, 1\}^{G \times n}$, where G is the total number of genes under consideration and n is the number of samples (from patients with and without cancer, to which we refer to as tumor samples

and normal samples, respectively). Each row corresponds to a gene and each column to a sample, i.e., $x_{g,s}$, the element in the g -th row and s -th column of X is set to 1 if the sample s has a mutation in the gene g (and 0 otherwise). We say a combination $\gamma = \{g_1, \dots, g_h\}$ of h genes, “covers” a particular sample s if *all* genes are mutated in sample s , i.e., $X_{g_1,s} = X_{g_2,s} = \dots = X_{g_h,s} = 1$. The set of samples covered by a single combination γ is denoted by:

$$\mathcal{C}(\gamma) = \{s : \forall g \in \gamma, x_{g,s} = 1\}, \quad (1)$$

while the set of samples covered by a set of combinations Γ is the union of the samples covered by the combinations in the set $\mathcal{C}(\Gamma) = \cup_{\gamma \in \Gamma} \mathcal{C}(\gamma)$.

As large-scale genomic data became widely accessible (spanning tens of thousands of genes in thousands of samples), finding the specific gene sets that constitute these multi-hit combinations became a computationally daunting task. Two primary solutions have emerged to address this challenge: (i) methods grounded in the weighted set cover (WSC) problem and (ii) graph-based approaches.

1) *Weighted Set Cover (WSC) Paradigm*: One of the most prominent solution strategies for multi-hit analysis is to formulate the problem as a weighted set cover (WSC) [7], [8], [19]. Here, the aim is to find a set of combinations with minimal weights that cover all tumor samples. That is, each combination γ has a weight $F(\gamma)$ associated with it, and the goal is to find the set of combinations Γ^* that has minimal combined weight among the sets that also covers the tumor samples.

Formally, denoting the set of all h gene combinations with Γ_h , the minimality objective can be stated as

$$F(\Gamma^*) = \min_{\Gamma \subset \Gamma_h} \{F(\Gamma)\} \quad \text{i.e.,} \quad \Gamma^* = \operatorname{argmin}_{\Gamma \subset \Gamma_h} \{F(\Gamma)\} \quad (2)$$

while $T \subset \mathcal{C}(\Gamma^*)$ expresses the fact that Γ^* covers the tumor samples, T (where, $\mathcal{C}(\Gamma) = \cup_{\gamma \in \Gamma} \mathcal{C}(\gamma)$).

a) *Scoring and Algorithmic Steps*: As an example of a WSC-based method, Dash et al. [19] maps the multi-hit problem to WSC and applies a greedy strategy to find sets of genes that appear *frequently* in tumor samples but *rarely* in normal samples. Formally, let $N_t(X)$ and $N_n(X)$ be the total number of tumor and normal samples, respectively. For each h -hit gene combination γ , $T_+(\gamma, X)$ is the number of tumor samples that contain *all* $g \in \gamma$ genes (true positives), and $T_-(\gamma, X)$ the number of normal samples that do *not* contain any of the h genes in the combination (true negatives).

A commonly used objective or “weight” function is [19]:

$$F(\gamma, X) = \frac{\alpha T_+(\gamma, X) + T_-(\gamma, X)}{N_t(X) + N_n(X)},$$

where α (often set to 0.1) penalizes the approach’s inherent bias toward maximizing T_+ over T_- . Until all tumor samples are covered, the algorithm, greedily selects the h -hit combination γ^* with the highest $F(\gamma, X)$ value, and removes the samples (i.e., columns) from X which are covered by γ^* as described by Algorithm 1.

Algorithm 1 Greedy Set Cover

Require: X gene mutation matrix, T indices of tumor samples, h number of hits

Ensure: Γ covers T , i.e., $T \subset \mathcal{C}(\Gamma)$

```
1:  $C \leftarrow \emptyset$  ▷ Set of covered samples
2:  $\Gamma \leftarrow \emptyset$  ▷ The variable holding the results
3: while  $C \subsetneq T$  do ▷ Are all tumors samples covered?
4:    $\gamma^* \leftarrow \operatorname{argmax}_{\gamma \in \Gamma_h} F(\gamma, X)$  ▷ Get the best combination
5:    $\Gamma \leftarrow \Gamma \cup \{\gamma^*\}$  ▷ Append  $\gamma^*$  to the results
6:    $C \leftarrow C \cup \mathcal{C}(\gamma^*)$  ▷ Update the set of covered samples
7:    $X \leftarrow \operatorname{DEL}(\operatorname{COLS}(X, \gamma^*))$  ▷ Remove samples from  $X$ 
8: end while
9: return  $\Gamma$ 
```

b) Computational Complexity: While straightforward in concept, enumerating *all* possible h -gene sets in line 4 of Algorithm 1 is computationally costly. The total number of h -gene combinations is $M = \binom{G}{h}$, where G is on the order of 20,000 genes. Even for $h = 4$, $M \approx 7 \times 10^{15}$, making an exhaustive search prohibitive. Formally, WSC is an NP-complete problem with no known polynomial-time exact solution [7]. Approximate or greedy algorithms reduce the worst-case complexity to $O(M \times N_t)$, which is still tractable only for small h . Thus, early multi-hit approaches using WSC focused on 2-hit or 3-hit gene sets, and more recent GPU-accelerated methods extended these analyses up to 5 hits [7], [8], [20]. However, jumping to 6-hit combinations (much less 8 or 9) remains largely infeasible via exhaustive enumeration or naive greedy methods.

c) Pruned and Parallel DFS for Candidate Generation: A common way to mitigate the $\binom{G}{h}$ blowup is to treat Γ_h as an implicit search tree and traverse it with depth-first search (DFS), while pruning subtrees that cannot yield useful candidates. This idea is well established in frequent itemset mining: DFS-style enumeration of h -way co-occurrences is paired with anti-monotone bounds to prune away large portions of the candidate lattice [21]–[23]. At scale, these DFS/backtracking trees are routinely parallelized by partitioning the search space (often by prefixes) and using dynamic load balancing like randomized work donation or work stealing, to handle highly irregular subtree sizes [24]–[26]. In the same spirit, our approach uses a pruned, parallel DFS to generate and score only promising h -hit candidates, rather than explicitly materializing all of Γ_h . Although exact set-cover solvers can use Branch and Bound (B&B) with relaxation-based bounds for safe pruning, we do not use B&B because our WSC-style greedy routine does not maintain such bounds [27].

2) Graph-Based Representations: While WSC aims to enumerate combinations explicitly, graph-based methods, such as BiGPICC [9], represent genomic data in the form of bipartite networks with gene nodes on one side and sample nodes on the other. Edges exist only if a gene is mutated in a given sample. Clustering algorithms (like the Leiden method [28]) then aim to group genes that frequently co-occur across patients.

a) Speed vs. Coverage: Graph-based strategies often reduce computational costs compared to full or partial enumerations. By clustering co-mutated genes, they can efficiently highlight general mutation patterns across large datasets. However, the trade-off is that crucial mutations may be missed when aggregated into clusters, which as a result, affects the classification accuracy as compared to the WSC approach. Thus, graph-based solutions are often preferred for quick large-scale screening or when fewer computational resources are available, but they may miss subtle “needle-in-a-haystack” multi-hit combinations.

III. PRUNED DEPTH-FIRST SEARCH (P-DFS): PRUNING ALGORITHM FOR h -HIT GENE MUTATIONS

A. Motivation

Our goal is to discover multi-hit gene combinations efficiently—in a reasonable amount of time—without sacrificing accuracy. We therefore build on the WSC paradigm, which directly optimizes tumor/normal discrimination rather than relying solely on graph clustering, which may blur the sample-level signal, and focus our contribution on shrinking the otherwise exhaustive h -hit candidate search space (via sparsity-driven pruning) while keeping the WSC scoring objective unchanged.

The first empirical observation motivating our design is the fact that the main loop in Algorithm 1 is executed at most a tens of times. More concretely, in datasets studied by prior work, the greedy cover typically terminated in ≤ 20 iterations [8], [19]. The program spends most of its time executing the greedy maximum search in step 4, so optimizing this step automatically improves the performance of the whole application. Another key observation behind the motivation is the extreme sparsity of somatic-mutation matrices. Most entries are zero: each tumor harbors alterations in only a small subset of genes, and each gene is altered in only a small subset of tumors. This “few mountains, many hills” profile and pathway-level mutual exclusivity have been extensively documented in cancer genomics [29]. Our datasets follow the same pattern, where the median sparsity is 95.61% (Fig. 3), which immediately suggests algorithmic opportunities.

The challenge in the original WSC approach is the combinatorial growth: the number of h -hit candidates scales as $\binom{G}{h}$, so even modest increases in h cause an explosion in the search space. Table I shows the number of h -gene candidates, $\binom{G}{h}$ and the corresponding cancers which require that number of gene hits for diagnosis. Even a one-hit increase yields orders of magnitude more combinations, making naive enumeration intractable (calculated here for $G=20,000$ genes). Naively enumerating all combinations to retain WSC’s accuracy becomes computationally intractable.

Our approach is to exploit sparsity to prune the search space and hence tame the combinatorial explosion while retaining WSC’s accuracy. Specifically, we structure the computation around early-termination bounds that prune branches as soon as partial intersections go empty. This would leverage the fact that true co-occurrences are rare, so most computation paths

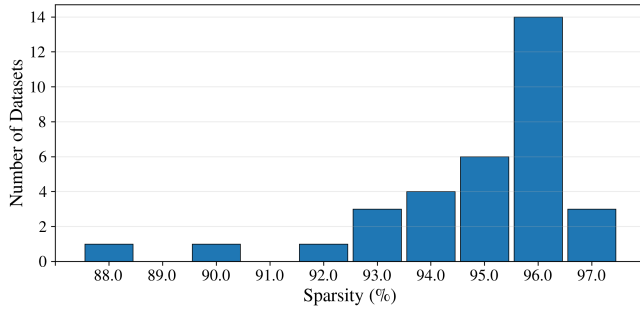


Fig. 3: Measured sparsity of all the carcinogenesis mutation matrix datasets available through TCGA. Median: **95.61%**. High sparsity underscores the rarity of mutations in all of the cancer datasets.

TABLE I: Combinatorial explosion of the WSC search space.

Hits	Combinations	Cancers
2	1.99×10^8	GBM, OV, UCEC
3	1.33×10^{12}	KIRC, LUDA, SKCM, COAD, BRCA
4	6.66×10^{15}	BLCA, HNSC
5	2.66×10^{19}	THCA, STAD, CESC, LUSC
6	8.88×10^{22}	LGG
7	2.53×10^{26}	DLBC, PRAD, ESCA
8	6.34×10^{29}	SARC, KIRP, LIHC
9	1.40×10^{33}	UCS, UVM, KICH, MESO, AC, PCPG

die quickly, leaving only a small collection of promising sets to evaluate thoroughly.

B. Overview

The workflow of our method consists of several key stages. First, we reorder the binary mutation matrix by gene sparsity, sorting rows from most to least sparse. This sparsity-aware preprocessing enables P-DFS to more effectively prune the search space when identifying candidate multi-hit combinations. To ensure efficient parallelization and workload distribution across MPI ranks, we employ a hierarchical work-stealing strategy (as illustrated in Fig. 4).

C. Preprocessing

We represent each cohort as a binary mutation matrix with genes as rows and samples as columns (tumor and normal samples are tracked distinctly; see Fig. 5 for an overview of the workflow). To accelerate P-DFS, we order gene rows from most sparse to least sparse prior to computation. This sparsity-aware ordering helps the search prune aggressively: combinations built from genes that show high sparsity in their mutations can get pruned early, thereby reducing the size of the explored sub-tree. In practice, this simple reordering decreases the number of combination intersections we must evaluate before a branch is pruned.

To make set operations fast, we represent each gene’s samples as a bit-vector and implement primitive operations

like intersection, union, and membership count via bitwise operations. This design helps by slashing the memory footprint, hence improving cache residency of hot rows.

D. Core Algorithm

As discussed in §II-B1b, the bottleneck of the algorithm is traversing all the h -hit gene combinations. Instead of scanning the entire search space, we restructure the traversal where for each λ , we perform a depth-first expansion with backtracking that prunes as soon as a partial intersection becomes empty. To effectively enable this solution, as mentioned in §III-C, we sort the gene rows by *increasing sparsity* (i.e., from most zero entries to fewer) to trigger empty partial intersections earlier.

For a growing partial set g_1, \dots, g_ℓ we maintain the running intersection $y_\ell \leftarrow x_{g_1} \wedge \dots \wedge x_{g_\ell}$ over the tumor cohort (bitwise AND). If at any step $y_\ell = \mathbf{0}$ (no tumor sample has all ℓ mutations), we immediately backtrack. There is nothing left to gain by adding more genes on that path, so the entire subtree can be skipped without evaluation. When we reach depth h with $y_h \neq \mathbf{0}$, we score γ via the objective $F(\gamma, X)$ and update the current best (F^*, γ^*). This simple rule is powerful in sparse data: many branches become empty after just a few ANDs, so we examine far fewer than $\binom{G}{h}$ combinations. The P-DFS approach does not change the worst-case time complexity of the original WSC search. In other words, if no branch ever empties, it degenerates to full enumeration of $\binom{G}{h}$ combinations. The algorithm simply aggressively prunes the search space in typical sparse cohorts, so the effective number of candidates evaluated (and the wall time) drops substantially.

The control flow is made explicit in Algorithm 2: the inner grow-and-check loop maintains the running intersection, and the early-exit test at line 7 performs the pruning.

E. Work Distribution: Scaling and Load Balancing

Our search space grows combinatorially with the number of genes and the hit depth, so we must expose massive concurrency. A naive partition by the first gene yields about 20,000 tasks for 20,000 genes and caps useful parallelism near 20,000 compute units. Instead, we flatten the nested loops over g_1 and g_2 into a single λ index so each (g_1, g_2) pair is an independent task (Fig. 5, ②), producing $C_2^G \approx \binom{20,000}{2}$ tasks—enough even at the exascale. Furthermore, pruning makes traversal cost per task highly *irregular*: some subtrees collapse after only a few intersections while others survive and expand. Equal counts of λ s therefore do not imply equal work, and a static partition risks idle ranks and stragglers. This motivates the MPI-based, dynamically assigned work distribution described below (see the control-flow overview in Fig. 4).

a) *MPI Execution Model and Data Residency*: We scale with MPI, running one rank per physical core, and assign disjoint λ sub-intervals to each rank for independent computation. Given that the dataset is just a few megabytes in size, each rank holds the entire input table. Furthermore, each rank obtains a subinterval of λ s from $[1, \dots, C_2^G]$. By decoding λ back to (g_1, g_2) , the state of the program corresponds to step 7 in

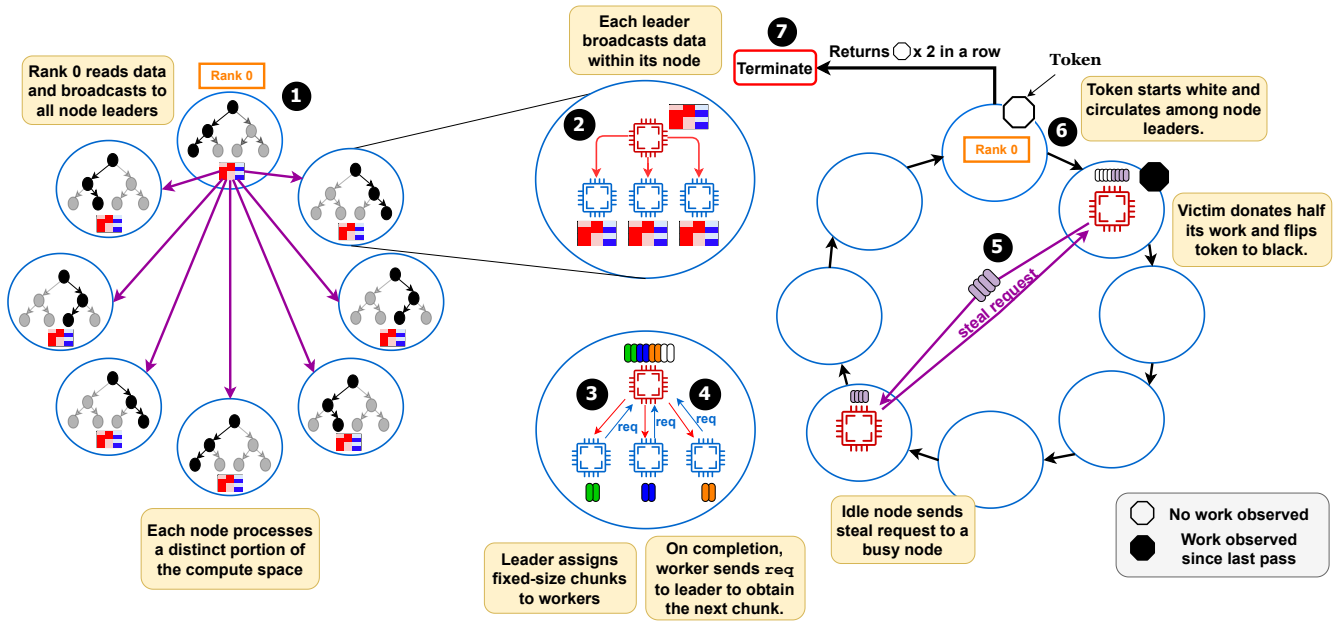


Fig. 4: **Work Distribution Overview:** We use one MPI rank per core and two communicators: a global communicator among node leaders and a local communicator within each node. The local Rank 0 of each node is the node leader and also belongs to the global communicator. ① Because the database is only a few MB, Rank 0 reads it from disk and broadcasts the entire database to all node leaders. Each node then computes a distinct subset of λ values, i.e., parallelism is in compute. ② Each node leader broadcasts the data within its node via the local communicator. ③ The leader tracks outstanding λ values and hands out fixed-sized work chunks to the workers. ④ When a worker finishes its portion of the compute, it sends a short `req` to the leader. If work remains, the leader issues another chunk, otherwise the worker becomes idle. ⑤ If a leader exhausts its local queue, it randomly selects a peer to steal from. A busy victim donates roughly half of its remaining range to the thief, while an idle peer triggers a retry with another node. ⑥ Termination is decided with a circulating token that starts at Rank 0 in the *white* state (no work observed) and moves around leaders in ring order. Any node that performs work or donates flips the token to *black* (work observed). ⑦ If the token returns to Rank 0 as black, it is reset to white and circulated again. If it returns white twice in a row, all the work to be computed on has been distributed, and a termination signal is sent.

Algorithm 2, and it can proceed to the first level of pruning if no samples share the mutations of both genes.

b) *Baseline: centralized master-worker:* We begin with a master-worker design in which rank 0 is the master and all other ranks are workers. The master maintains a single global pool of λ indices and dispenses fixed-size chunks with indices $\langle \text{start}, \text{end} \rangle$ on demand. Each worker stores only the bounds of its current chunk, computes directly over its private copy of the table, and, upon completion, sends a short request to the master for the next chunk. Using a fixed chunk size keeps assignment constant-time and minimizes bookkeeping, so control traffic remains light. In other words, workers communicate only when pulling new work and when receiving the final termination signal from the master.

c) *Limitations of centralized master-worker:* A single global master would saturate on large machines. Every request would target one rank, queues would grow, and the MPI progress engine would spend time on control traffic rather than computation. Prior studies of dynamic scheduling report that single point task coordination limits scalability and motivates multi-level coordinators [30], [31]. We therefore move to a hierarchical organization that respects the machine topology.

d) *Topology-aware hierarchical organization:* All ranks on a node form a local communicator and designate rank 0 as the node leader. All node leaders form a second communicator that spans nodes. Leaders manage work inside the node, and coordinate only coarse actions across nodes, which reduces cross-node traffic and removes the single choke point.

e) *Two-level work stealing:* Work stealing operates at two levels. Inside a node, workers never steal from each other. They always ask the node leader for the next interval. Across nodes, leaders both request and donate work. When a leader runs out of local work it selects a peer leader and issues a steal request. Peer selection is randomized with a small number of retries in case the chosen leader has no more work to give. This spreads requests across the ring of leaders and avoids hot spots. When a leader receives a steal request it answers from its own remaining interval. The leader replies with the upper half of its remaining λ -interval. This splits its workload roughly in two, hands a single contiguous block, which is essentially a $\langle \text{start}, \text{end} \rangle$ interval, to the thief. The victim also records that a donation occurred via a local flag, which is used later during coordination.

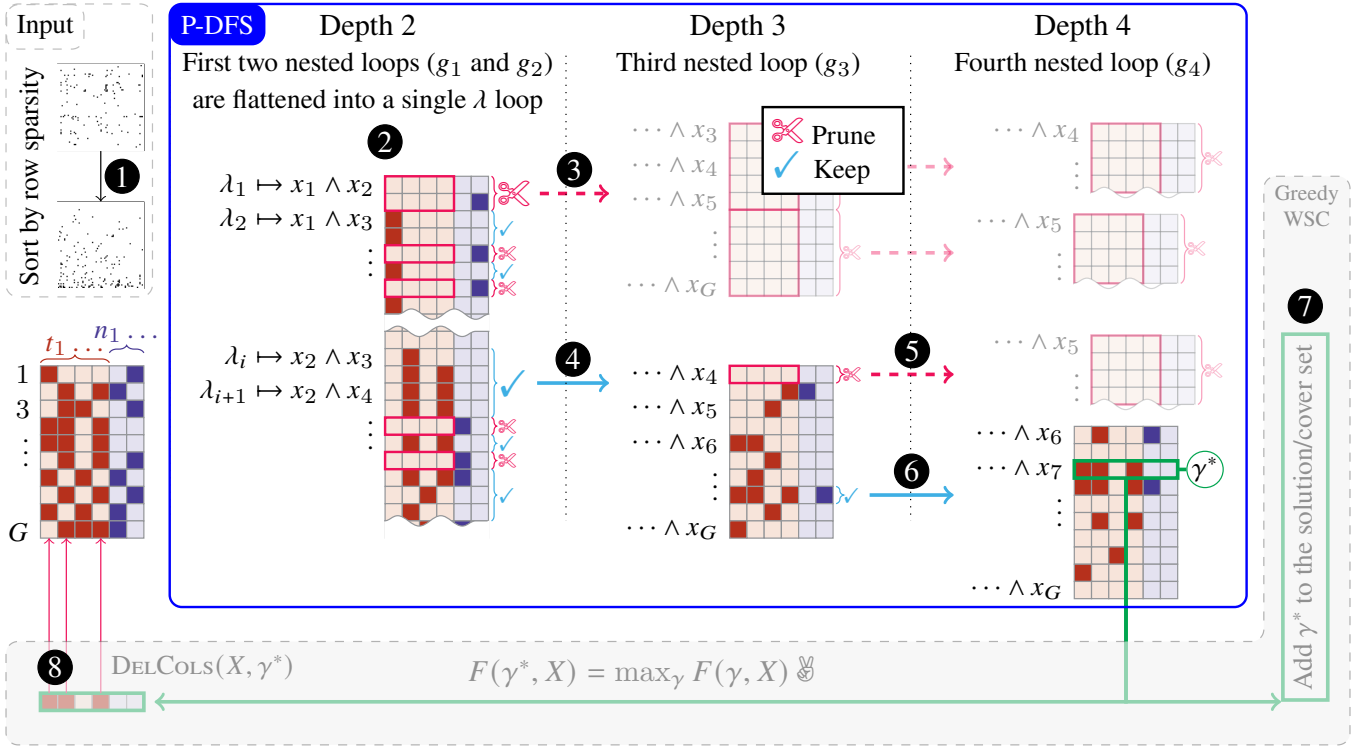


Fig. 5: **Pruned depth-first search (P-DFS): pruning algorithm for h -hit gene mutations** (with $h = 4$): In the preprocessing step, the input data is sorted ① based on row sparsity to improve pruning efficiency. The first two of the four nested loops, with iterators g_1 and g_2 are flattened into a single λ -loop ② to enable work distribution with a high number of workers. In each iteration of the λ -loop the partial combination using only rows g_1 and g_2 are computed. If all the tumor samples are zero/false, the combination cannot contribute to the set cover (empty cover), nor would the resulting, higher hit combinations, so the entire subtree can be skipped ③. Otherwise, the algorithm proceeds to the depth 3 nested loop ④ of the search tree, computing the 3-hit combination (using the 2-hit partial results) and similar eliminates empty covers ⑤ or proceeds to depth 4 as needed ⑥. The γ^* combination with the best $F(\gamma, X)$ value is saved ⑦ and the samples (columns) covered by it are removed ⑧ from the input database for the next iteration.

f) *Barrier-free termination detection*: Termination and global progress use a token on the leader communicator. Leaders form a logical ring. The root creates a white token and sends it to the next leader. A leader forwards the token only when it is idle and has no local work, and if it has donated work since it last saw the token it turns the token black before forwarding. If the root receives a white token twice in succession while it is idle, there is no outstanding work. The root then sets the termination flag via MPI one-sided communication, issuing an `MPI_Put` into a shared RMA window, and each leader notifies its workers to exit their request loop. This protocol detects quiescence without a global barrier and remains robust under random steals, since the black color records backward donations and suppresses premature termination.

g) *Hierarchical collectives: Broadcast and AllReduce*: Reductions and broadcasts follow an identical hierarchy structure. First, within each node, processes reduce onto a designated leader using intranode collectives that exploit shared memory. The leaders then perform the internode collective on the leader communicator. Finally, each leader distributes the result back to its local workers via an intranode broadcast.

Although this hierarchical framework increases memory consumption, it reduces message traffic on the network fabric and shortens the critical path for large collectives, which is crucial on systems where MPI buffers and progress threads face significant contention at scale (realistic benchmarks demonstrate up to a $7\times$ speedup for all-reduce using these two-level structures compared to standard `MPI_Allreduce`).

h) *Communication profile and the MPI-only choice*: Given that we replicate the gene-sample mutation table per rank, all the inner loop work memory stays local to the node and communication is confined to work requests, inter-leader steals, hierarchical collectives, and a final termination flag. We prefer rank-per-core over hybrid MPI+OpenMP for this irregular, fine-grained workload because thread schedulers introduce overheads from frequent returns to the scheduler, extra barriers, and affinity or NUMA pitfalls, which can make hybrid slower than pure MPI without careful tuning [32], [33].

F. Pre-sorted DFS Finds Smaller Covers at Higher Hit Thresholds

An advantage of our algorithm is that it yields better solutions, i.e., smaller set covers, at higher hit thresholds.

Algorithm 2 P-DFS: Implementing step 4 of Algorithm 1 as a depth-first maximum search with backtracking.

Require: X gene mutation matrix, h number of hits

Ensure: $\gamma^* = \operatorname{argmax}_{\gamma \in \Gamma_h} F(\gamma, X)$

```

1:  $F^* \leftarrow -\infty$  ▷ Initialize maximum search
2: for  $g_1 = 1$  to  $G - h + 1$  do ▷ Depth 1
3:    $\gamma \leftarrow g_1$  ▷ The  $g_1$ -th row of  $X$ 
4:   for  $g_2 = g_1 + 1$  to  $G - h + 2$  do ▷ Depth 2
5:      $\gamma \leftarrow \gamma \cup g_2$  ▷ Implemented as element-wise
     logical AND
6:     if  $x_{g_1} \wedge x_{g_2} = 0$  then
7:       continue ▷ Eliminate branch
8:     end if
9:     ...
10:    for  $g_h = g_{h-1} + 1$  to  $G$  do ▷ Depth  $h$ 
11:       $\gamma \leftarrow \gamma \cup \{g_h\}$ 
12:       $F \leftarrow F(\gamma, X)$ 
13:      if  $F > F^*$  then ▷ Maximum search
14:         $F^* \leftarrow F$ ;  $\gamma^* \leftarrow \gamma$ 
15:      end if
16:    end for
17:    ...
18:  end for
19: end for
20: return  $\gamma^*$ 

```

TABLE II: Comparison of Proposed Algorithm vs. Original WSC Solution Size for Various Cancers and Hit Sizes

Cancer	Hit Size	Proposed Algorithm	Original WSC
BLCA	2	17	15
GBM	2	11	N/A
OV	2	9	N/A
UCEC	2	5	9
BLCA	3	16	12
BRCA	3	12	8
COAD	3	12	10
KIRC	3	9	6
LUAD	3	13	10
SKCM	3	11	N/A
BLCA	4	16	19
HNSC	4	13	17

As shown in Table II, with our algorithm we reduce the solution size at four hits by 80% average. Since the size of the solution space grows exponentially with the number of hits, obtaining smaller cover sets at higher number of hits provides a substantial performance benefit, as the search can terminate earlier once a minimal cover is found. In this section, we analyze why the proposed algorithm tends to produce smaller cover sets at higher hit thresholds.

As introduced in Eq. (2), our goal is to find the set of combinations that has a minimal combined weight. While the baseline explores combinations randomly, the proposed

algorithm sorts genes, i.e. matrix rows, by sparsity (from fewer to more mutations), and uses P-DFS to prune the search space of combinations.

1) *Effect of sparsity at high h :* When the number of hits h is small (e.g., $h = 2$), dense genes with many mutations quickly increase the hit coverage \mathcal{C} defined in Eq. (1) even if they overlap strongly. At higher h , however, overlapping dense genes provide less new information, because many samples already share the same mutations. Thus, the expected marginal gain of a gene g given the current partially constructed combination of genes γ , $\Delta_h(g | \gamma) = \mathcal{C}(\gamma \cup \{g\}) - \mathcal{C}(\gamma)$, decreases more sharply for dense genes as h increases. Sparse genes, which cover fewer but more distinct samples, maintain higher marginal gain when h is large.

2) *Pruning advantage:* Because our search visits sparse genes first, partial solutions grow coverage efficiently with minimal redundancy. This makes the upper bound on remaining possible gain, $U_h(\gamma) = \max_{S \subseteq \Gamma_h \setminus \gamma} \mathcal{C}(\gamma \cup S) - \mathcal{C}(\gamma)$, drop faster as the search deepens. Branches that cannot reach the target are pruned earlier. At higher h , the redundancy among dense genes strengthens this effect, reducing the effective branching factor and shrinking the explored tree from $O(2^n)$ toward $O(2^L)$, where L is the number of sparse, high-value genes.

3) *Resulting behavior:* This explains why the proposed method produces smaller covers at $h = 4$. For large h , sparse-first ordering better matches the structure of the residual samples, yields higher marginal gains per added gene, and enables tighter pruning. In contrast, random or dense-first exploration revisits many redundant regions, leading to larger covers or slower convergence. Empirically, this aligns with our results, where P-DFS achieves smaller solution sizes at 4-hit thresholds.

IV. RESULTS AND DISCUSSION

A. Experimental Platform: Fugaku

All experiments were conducted on the supercomputer Fugaku, located in Kobe, Japan. Each node contains a single Fujitsu A64FX processor with 48 compute cores and 32 GB of HBM2 memory. We use Fujitsu MPI and run one MPI rank per core with no intra-rank threading. This choice avoids thread-scheduler overheads and lets each rank maintain a private copy of the data. Our datasets are only a few megabytes per cohort, so replication across 48 ranks comfortably fits within the 32 GB node memory budget and removes contention on shared data structures.

Nodes are connected by the Tofu-D interconnect in a six-dimensional mesh-torus topology. We request compact allocations that form near-cubic sub-tori so that the job spans similar extents in each of the six dimensions. This placement reduces average hop distance, preserves bisection bandwidth, and helps keep collective and point-to-point costs stable as we scale out. The node counts in our strong-scaling studies $\{192, 384, 768, 1,536, 3,072\}$ were chosen because they tile the 6D topology cleanly and allow the scheduler to pack jobs contiguously.

Our MPI configuration follows the algorithmic design. A single leader rank per job performs interval assignment, and all other ranks act as workers that compute against their private tables. We bind one rank to one physical core and pin memory locally to improve cache residency on A64FX. Communication consists of short messages to pull work and a few global notifications at the end of the run. On Tofu-D these messages traverse few hops under compact placement, which keeps the communication term nearly constant across scales, as observed in §IV-F. The combination of rank-per-core, data replication, and compact topology-aware placement is what allows the pruned workload to remain compute dominated over a wide range of node counts.

B. Dataset

Somatic mutation data in the Mutation Annotation Format (MAF) was acquired from The Cancer Genome Atlas (TCGA) [34]. All mutations were identified via the Mutect2 software, a commonly utilized tool in the genomic community. Each cancer type was processed individually, extracting gene-level mutations paired with patient sample identifiers. Silent mutations were excluded to focus on potentially functional variants. Following preprocessing, each dataset was divided into train and test sets at 75% and 25%, respectively.

C. Pruning Efficiency and End-to-End Runtime

A central outcome of our approach is that we only visit a tiny fraction of the potential h -hit combinations. For each cohort, we tracked the exact number of combinations that the P-DFS traversal evaluated and compared it to a non-pruning baseline whose search space equals the combinatorial maximum $\binom{20,000}{h}$. Cohorts are paired with the hit sizes reported in [3], which estimates the number of hits for 17 cancer types with at least 200 samples.

Fig. 6 reports, for multiple cohorts and hit sizes, the normalized number of combinations that are actually visited by our algorithm. The blue bars represent the total search space and are normalized to 1.0 by construction. The orange bars show the fraction we visit. Lower orange bars indicate more pruning. We observe a consistent drop in visitation as h increases. This behavior is expected because early intersections become empty much more often at higher h . In sparse mutation matrices, the probability that a sample carries all genes in a growing partial set decreases rapidly with each added gene. The result is aggressive pruning at higher hit sizes and a dramatic reduction in evaluated candidates.

Pruning translates directly into wall-time gains. We study this effect with a 4-hit run for BLCA across 192, 384, 768, 1,536, and 3,072 nodes. We also plot an ideal strong-scaling line for the pruned workload to check whether runtime falls in inverse proportion to node count. For a fixed workload of size MN_t the ideal time on N nodes is $T_{\text{ideal}}(N) = \frac{cMN_t}{N}$, where M is the number of combinations actually visited by the algorithm, N_t is the number of tumor samples, and c is a platform constant that captures per-combination cost. We

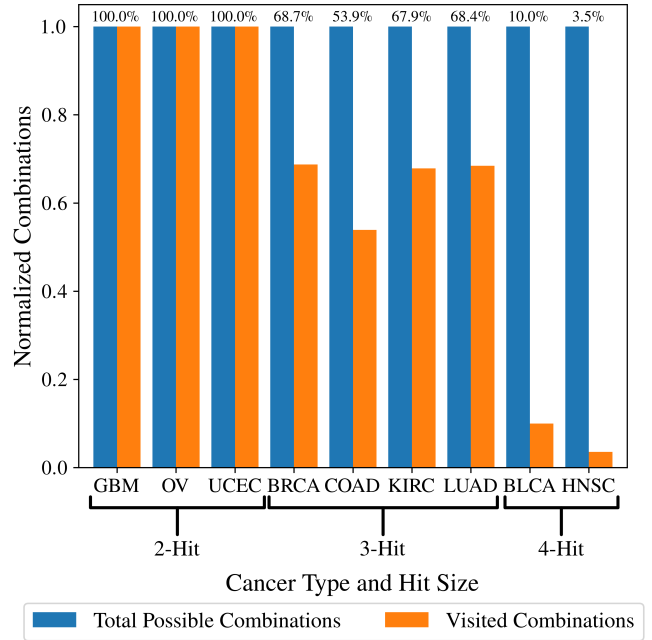


Fig. 6: Pruned search vs. theoretical maximum. For each cohort and hit size, the total combinations $\binom{20,000}{h}$ are normalized to 1.0 (blue). The orange bars show the fraction of combinations actually visited by our sparsity-driven P-DFS method.

calibrate c from the 192-node run, $c = \frac{T_{\text{measured}}(192) \cdot 192}{MN_t}$, which yields $T_{\text{ideal}}(N) = T_{\text{measured}}(192) \cdot \frac{192}{N}$.

The bounded curve lies close to this line up to 768 nodes but shows slight divergence beyond 768 nodes.

To highlight the value of pruning, we also executed a baseline run at 3,072 nodes. This job did not finish within the four-hour allocation. Based on the completed portion, we estimate a time to solution of about 52 hours on 3,072 nodes. This projected time is much slower than the P-DFS method even at 192 nodes. The gap reflects the massive volume of candidates that fail the first few intersection checks and yet must still be evaluated when pruning is disabled.

Taken together, Figs. 6 and 7 show that our design delivers much better performance compared to the brute-force weighted set cover algorithm. The algorithm prunes vast regions of the search space before computing the weights.

D. Accuracy on Held-out Data

We evaluate accuracy of the P-DFS method with a random 75%–25% train–test split per cohort. On the training set, the algorithm learns a small set of h -hit gene combinations using P-DFS weighted set cover method. We then freeze those combinations and assess coverage on the disjoint Test set. For each cohort we report:

- **Tumor Covered:** number of tumor samples that contain at least one learned h -hit combination.
- **Normal Covered:** number of normal samples that contain at least one learned h -hit combination.

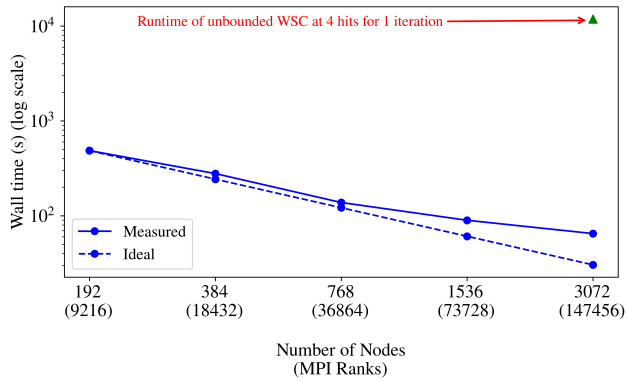


Fig. 7: **Wall time vs. scale for 4 hits.** Measured wall times for the P-DFS runs across nodes, together with the ideal strong-scaling line.

TABLE III: Training split (75%). Tumor and normal coverage and derived sensitivity/specificity for learned combinations.

Cancer	Hits	TC	TT	NC	NT	Sens.	Spec.
BLCA	4	309	309	0	248	1.0	1.0
HNSC	4	382	382	0	248	1.0	1.0
BLCA	3	309	309	0	248	1.0	1.0
BRCA	3	786	786	8	248	1.0	0.9677
COAD	3	325	325	4	248	1.0	0.9839
KIRC	3	288	288	1	248	1.0	0.9960
LUAD	3	426	426	0	248	1.0	1.0
SKCM	3	352	352	0	248	1.0	1.0
GBM	2	297	297	0	248	1.0	1.0
OV	2	319	319	2	248	1.0	0.9919
UCEC	2	406	406	8	248	1.0	0.9677
BLCA	2	309	309	0	248	1.0	1.0

a) *Training performance:* Table III summarizes results on the training split (TC, TT, NC, NT, Sens. and Spec. correspond to number of covered tumor samples, total number of tumor samples, number of covered normal samples, total number of normal samples, sensitivity and specificity, respectively). Sensitivity is 1.0 for all cohorts, and specificity is very high, with small leakage into normals for BRCA, COAD, KIRC, OV, and UCEC. These results are expected because the model is optimized on the training set. Furthermore, these values represent an upper bound on achievable performance for a given h .

b) *Generalization:* Table IV reports performance on the disjoint 25% test split using the combinations learned on training (column names detailed in §IV-D0a). Sensitivity remains high across cohorts (0.85–0.98), and specificity is similarly strong (0.81–0.99). The small reduction relative to training reflects that some held-out tumors lack the exact h -hit patterns selected during training.

c) *Takeaways:* Across ten cohorts and hit sizes guided by [3], our approach achieves near-perfect sensitivity and very high specificity on training, and maintains strong accuracy on

TABLE IV: Held-out Test split (25%). Coverage-based sensitivity and specificity using combinations learned on the Training split.

Cancer	Hits	TC	TT	NC	NT	Sens.	Spec.
BLCA	4	88	103	16	83	0.8544	0.8072
HNSC	4	113	128	14	83	0.8828	0.8313
BLCA	3	89	103	12	83	0.8641	0.8554
BRCA	3	257	262	13	83	0.9809	0.8434
COAD	3	97	109	8	83	0.8899	0.9036
KIRC	3	92	97	8	83	0.9485	0.9036
LUAD	3	124	143	14	83	0.8671	0.8313
SKCM	3	106	118	7	83	0.8983	0.9157
BLCA	2	88	103	6	83	0.8544	0.9277
GBM	2	95	99	1	83	0.9596	0.9880
OV	2	102	107	3	83	0.9533	0.9639
UCEC	2	131	136	5	83	0.9632	0.9398

test data. High test sensitivity indicates that the selected h -hit patterns capture tumor signal that generalizes to unseen patients. High test specificity shows that normal tissue rarely matches these patterns. Combined with the pruning and scaling results, these accuracy outcomes demonstrate that the algorithm is biologically discriminative at scale.

E. Load Balancing and the Impact of Work Stealing

We quantify the effect of irregularity by measuring the worker running time on BLCA with 4 hits at 1,536 nodes. Worker running time records only periods when a worker is computing, not idle or waiting on the leader. We run the same configuration with work stealing enabled and disabled and collect per-worker histograms.

Fig. 8 shows the distributions. Without stealing the distribution is broad with heavy right tails, which indicates that many workers receive subtrees that are much larger than average. With stealing the distribution collapses into a sharp peak. The standard deviation drops from 544.186 seconds without stealing to 41.9599 seconds with stealing, a $13\times$ reduction in spread. Likewise, **we observed average worker idleness likewise falls from 63.61% (no stealing) to 22.31% (with stealing), reinforcing the benefits of work stealing.** This indicates that workers finish at nearly the same time when stealing is enabled. The reduced spread and average idleness of the workers aligns with the lower wall times reported in Fig. 7, since long stragglers can dominate end-to-end time.

F. Strong Scaling Across Hit Sizes

We now quantify the parallel efficiency across hit sizes using speedup from a 192-node baseline. For each cohort we keep the algorithm and implementation fixed: P-DFS method with work stealing, and only vary the node count $N \in \{192, 384, 768, 1536, 3072\}$. A key trend stands out: scaling improves as the hit count increases, with BLCA (4 hits) tracking the ideal most closely, BRCA (3 hits) in the middle, and OV (2 hits) saturating early. Before interpreting

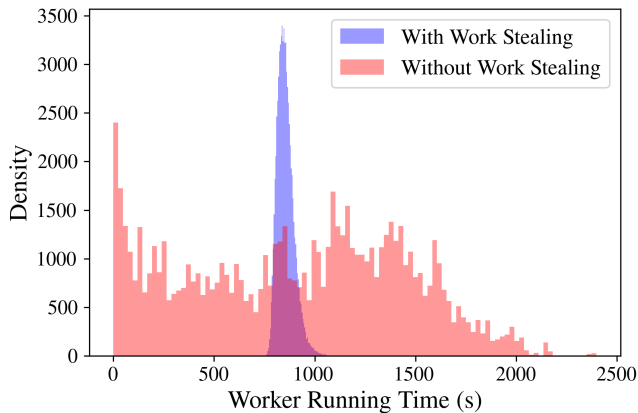


Fig. 8: Per-worker running-time distributions for BLCA, 4 hits, 1,536 nodes.

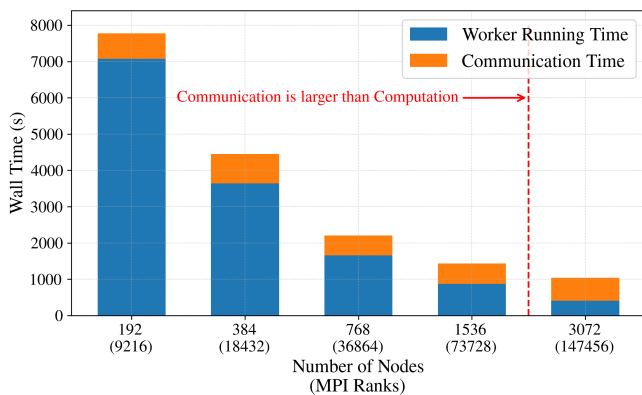


Fig. 9: Wall-time breakdown of BLCA at 4 hits.

the speedup curves, we first examine what fraction of wall time is computation versus communication.

Fig. 9 decomposes wall time into worker running time and communication for BLCA at 4 hits. Communication is comparatively constant across scales, while worker running time falls with node count as expected for a compute-dominated phase. When the compute term is large the constant is amortized and strong scaling holds. When the compute term is small the communication limits the additional speedup.

With this context we return to the speedup curves. After pruning, the useful work is proportional to MN_t , where M is the number of combinations actually visited and N_t is the number of tumor samples. A simple model $T(N) \approx \frac{cMN_t}{N} + T_{\text{comm}}$ explains the observations. For low hit counts, M is small because intersections go empty early, so $\frac{cMN_t}{N}$ becomes comparable to the constant T_{comm} at modest N . The OV (2-hit) curve therefore plateaus and even dips as noise and fixed overheads dominate. As the hit count increases, more combinations survive pruning, so M is larger and the compute term dominates over a wider range of N . BRCA (3 hits) improves over OV, and BLCA (4 hits) stays close to the ideal line because the run remains compute bound even at 3,072 nodes.

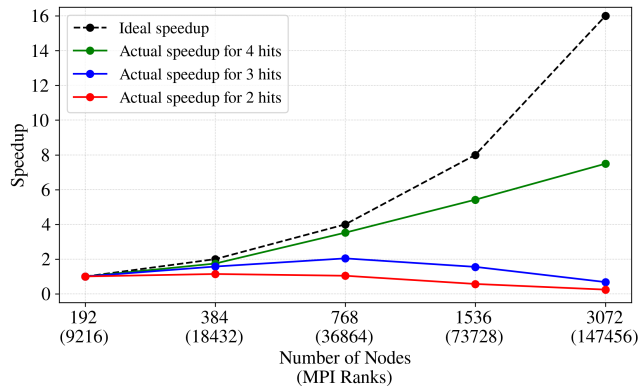


Fig. 10: Strong scaling speedup from 192 to 3,072 nodes for BLCA 4-hit, BRCA 3-hit, and OV 2-hit datasets.

V. CONCLUSION

We present a sparsity-aware depth-first search algorithm with backtracking that serves as our main contribution: a pruning technique for the weighted set cover (WSC) pipeline, called *pruned depth-first search*, for discovering multi-hit gene combinations. By sorting genes by sparsity, maintaining running bitset intersections, and backtracking as soon as partial covers are found to be empty, the search algorithm discards vast swaths of the combinatorial space (i.e., reduces the candidate search space) before scoring with the (standard) WSC selection step. To expose parallelism, we flatten the first two nested loops of the WSC algorithm into a single λ index and distribute contiguous $\langle \text{start}, \text{end} \rangle$ intervals, enabling high worker counts. A hierarchical MPI design, with per-node leader, lightweight request/response assignment, and barrier-free termination, keeps control traffic low and avoids single-master bottlenecks.

Empirically, pruning grows more effectively with the hit threshold. In other words, higher h induces emptier partial intersections, shrinking the visited space and reducing wall time relative to exhaustive WSC enumeration. On Fugaku, we observe that strong scaling improved as we increase the number of hits being computed. Furthermore, we observe tighter load-balance distributions when hierarchical scheduling is enabled. Across cohorts, the resulting combinations achieve high sensitivity and specificity on held-out data (via random 75%–25% splits), indicating that sparsity-driven pruning, paired with weighted set-cover scoring yields patterns that generalize. Taken together, these results demonstrate that P-DFS pruning converts an otherwise intractable enumeration into a high-throughput search at scale.

CODE AVAILABILITY

The reference implementation and scripts to reproduce our results are available at <https://github.com/RitvikPrabhu/P-DFS-Multihit-WSC>.

ACKNOWLEDGMENTS

We thank Niteya Shah for constructive comments and feedback on an early draft of this paper.

REFERENCES

- [1] J. S. Brown, S. R. Amend, R. H. Austin, R. A. Gatenby, E. U. Hammarlund, and K. J. Pienta, "Updating the Definition of Cancer," *Molecular Cancer Research*, vol. 21, no. 11, pp. 1142–1147, Nov. 2023. [Online]. Available: <https://doi.org/10.1158/1541-7786.MCR-23-0411>
- [2] R. L. Siegel, T. B. Kratzer, A. N. Giaquinto, H. Sung, and A. Jemal, "Cancer Statistics, 2025," *CA: A Cancer Journal for Clinicians*, vol. 75, no. 1, pp. 10–45, 2025. eprint: <https://onlinelibrary.wiley.com/doi/pdf/10.3322/caac.21871>. [Online]. Available: <https://onlinelibrary.wiley.com/doi/abs/10.3322/caac.21871>
- [3] R. Anandakrishnan, R. T. Varghese, N. A. Kinney, and H. R. Garner, "Estimating the Number of Genetic Mutations (hits) Required for Carcinogenesis Based on the Distribution of Somatic Mutations," *PLoS Computational Biology*, vol. 15, no. 3, p. e1006881, Mar. 2019. [Online]. Available: <https://www.ncbi.nlm.nih.gov/pmc/articles/PMC6424461/>
- [4] B. Al-Lazikani, U. Banerji, and P. Workman, "Combinatorial Drug Therapy for Cancer in the Post-Genomic Era," *Nature Biotechnology*, vol. 30, no. 7, pp. 679–692, Jul. 2012.
- [5] H. Ledford, "Cocktails for Cancer with a Measure of Immunotherapy," *Nature*, vol. 532, no. 7598, pp. 162–164, Apr. 2016, publisher: Nature Publishing Group. [Online]. Available: <https://www.nature.com/articles/532162a>
- [6] International Human Genome Sequencing Consortium, "Finishing the Euchromatic Sequence of the Human Genome," *Nature*, vol. 431, no. 7011, pp. 931–945, Oct. 2004, publisher: Nature Publishing Group. [Online]. Available: <https://www.nature.com/articles/nature03001>
- [7] S. Dash, Q. Al-Hajri, W.-c. Feng, H. R. Garner, and R. Anandakrishnan, "Scaling Out a Combinatorial Algorithm for Discovering Carcinogenic Gene Combinations to Thousands of GPUs," in *2021 IEEE International Parallel and Distributed Processing Symposium (IPDPS)*. Portland, OR, USA: IEEE, May 2021, pp. 837–846. [Online]. Available: <https://ieeexplore.ieee.org/document/94460537/>
- [8] Q. Al Hajri, S. Dash, W.-c. Feng, H. R. Garner, and R. Anandakrishnan, "Identifying Multi-Hit Carcinogenic Gene Combinations: Scaling up a Weighted Set Cover Algorithm Using Compressed Binary Matrix Representation on a GPU," *Scientific Reports*, vol. 10, no. 1, p. 2022, Feb. 2020, publisher: Nature Publishing Group. [Online]. Available: <https://www.nature.com/articles/s41598-020-58785-y>
- [9] V. Oles, S. Dash, and R. Anandakrishnan, "BiPICC: A Graph-Based Approach to Identifying Carcinogenic Gene Combinations from Mutation Data," Feb. 2023, pages: 2023.02.06.527327 Section: New Results. [Online]. Available: <https://www.biorxiv.org/content/10.1101/2023.02.06.527327v1>
- [10] A. G. Knudson, "Mutation and Cancer: Statistical Study of Retinoblastoma," *Proceedings of the National Academy of Sciences of the United States of America*, vol. 68, no. 4, pp. 820–823, Apr. 1971. [Online]. Available: <https://www.ncbi.nlm.nih.gov/pmc/articles/PMC389051/>
- [11] X. Zhang and R. Simon, "Estimating the Number of Rate Limiting Genomic Changes for Human Breast Cancer," *Breast Cancer Research and Treatment*, vol. 91, no. 2, pp. 121–124, May 2005. [Online]. Available: <https://doi.org/10.1007/s10549-004-5782-y>
- [12] C. Tomasetti, L. Marchionni, M. A. Nowak, G. Parmigiani, and B. Vogelstein, "Only Three Driver Gene Mutations are Required for the Development of Lung and Colorectal Cancers," *Proceedings of the National Academy of Sciences of the United States of America*, vol. 112, no. 1, pp. 118–123, Jan. 2015. [Online]. Available: <https://www.ncbi.nlm.nih.gov/pmc/articles/PMC4291633/>
- [13] M. P. Little and E. G. Wright, "A Stochastic Carcinogenesis Model Incorporating Genomic Instability Fitted to Colon Cancer Data," *Mathematical Biosciences*, vol. 183, no. 2, pp. 111–134, Jun. 2003. [Online]. Available: <https://www.sciencedirect.com/science/article/pii/S0025556403000403>
- [14] J. H. Bavarva, H. Tae, L. McIver, E. Karunasena, and H. R. Garner, "The Dynamic Exome: acquired variants as individuals age," *Aging (Albany NY)*, vol. 6, no. 6, pp. 511–521, Jun. 2014. [Online]. Available: <https://www.ncbi.nlm.nih.gov/pmc/articles/PMC4100812/>
- [15] X. Wu, E. D. Strome, Q. Meng, P. J. Hastings, S. E. Plon, and M. Kimmel, "A Robust Estimator of Mutation Rates," *Mutation Research/Fundamental and Molecular Mechanisms of Mutagenesis*, vol. 661, no. 1, pp. 101–109, Feb. 2009. [Online]. Available: <https://www.sciencedirect.com/science/article/pii/S0027510708003084>
- [16] L. B. Alexandrov, P. H. Jones, D. C. Wedge, J. E. Sale, P. J. Campbell, S. Nik-Zainal, and M. R. Stratton, "Clock-like Mutational Processes in Human Somatic Cells," *Nature genetics*, vol. 47, no. 12, pp. 1402–1407, Dec. 2015. [Online]. Available: <https://www.ncbi.nlm.nih.gov/pmc/articles/PMC4783858/>
- [17] Y. R. Paashuis-Lew and J. A. Huddle, "Spontaneous Mutation During Fetal Development and Post-Natal Growth," *Mutagenesis*, vol. 13, no. 6, pp. 613–617, Nov. 1998.
- [18] Wikiversity, "WikiJournal of Medicine/Medical Gallery of Mikael Häggström 2014 — Wikiversity," 2024, [Online]; accessed 25-September-2024. [Online]. Available: https://en.wikiversity.org/w/index.php?title=WikiJournal_of_Medicine/Medical_gallery_of_Mikael_H%C3%A4ggstr%C3%B6m_2014&oldid=2655064
- [19] S. Dash, N. A. Kinney, R. T. Varghese, H. R. Garner, W.-c. Feng, and R. Anandakrishnan, "Differentiating Between Cancer and Normal Tissue Samples Using Multi-Hit Combinations of Genetic Mutations," *Scientific Reports*, vol. 9, no. 1, p. 1005, Jan. 2019. [Online]. Available: <https://www.nature.com/articles/s41598-018-37835-6>
- [20] S. Dash, M. A. Haque Monil, J. Yin, R. Anandakrishnan, and F. Wang, "Distributing Simplex-Shaped Nested for-Loops to Identify Carcinogenic Gene Combinations," in *2023 IEEE International Parallel and Distributed Processing Symposium (IPDPS)*, May 2023, pp. 974–984, iSSN: 1530-2075. [Online]. Available: <https://ieeexplore.ieee.org/abstract/document/10177404>
- [21] C. Borgelt, "Frequent Item Set Mining," *Wiley Interdisciplinary Reviews: Data Mining and Knowledge Discovery*, vol. 2, no. 6, pp. 437–456, 2012.
- [22] T. Uno, T. Asai, Y. Uchida, and H. Arimura, "LCM: An Efficient Algorithm for Enumerating Frequent Closed Item Sets." in *Fimi*, vol. 90, 2003.
- [23] J. M. Luna, P. Fournier-Viger, and S. Ventura, "Frequent Itemset Mining: A 25 years review," *Wiley Interdisciplinary Reviews: Data Mining and Knowledge Discovery*, vol. 9, no. 6, 2019.
- [24] R. M. Karp and Y. Zhang, "Randomized Parallel Algorithms for Backtrack Search and Branch-and-Bound Computation," *Journal of the ACM*, vol. 40, no. 3, pp. 765–789, 1993.
- [25] R. D. Blumofe and C. E. Leiserson, "Scheduling Multithreaded Computations by Work Stealing," *Journal of the ACM*, vol. 46, no. 5, pp. 720–748, 1999.
- [26] K. Hiraiishi, M. Yasugi, S. Umatani, and T. Yuasa, "Backtracking-based Load Balancing," in *Proceedings of the 14th ACM SIGPLAN Symposium on Principles and Practice of Parallel Programming (PPoPP '09)*. ACM, 2009, pp. 55–64.
- [27] A. Caprara, M. Fischetti, and P. Toth, "Algorithms for the Set Covering Problem," *Annals of Operations Research*, vol. 98, pp. 353–371, 2000.
- [28] V. A. Traag, L. Waltman, and N. J. van Eck, "From Louvain to Leiden: guaranteeing well-connected communities," *Scientific Reports*, vol. 9, no. 1, p. 5233, Mar. 2019, publisher: Nature Publishing Group. [Online]. Available: <https://www.nature.com/articles/s41598-019-41695-z>
- [29] B. Vogelstein, N. Papadopoulos, V. E. Velculescu, S. Zhou, L. A. Diaz Jr, and K. W. Kinzler, "Cancer Genome Landscapes," *science*, vol. 339, no. 6127, pp. 1546–1558, 2013.
- [30] X. Yang, C. Liu, and J. Wang, "Large-Scale Branch Contingency Analysis Through Master/Slave Parallel Computing," *Journal of Modern Power Systems and Clean Energy*, vol. 1, no. 2, pp. 159–166, Sep. 2013. [Online]. Available: <https://ieeexplore.ieee.org/document/8939493/>
- [31] S. Perarnau and M. Sato, "Victim Selection and Distributed Work Stealing Performance: A Case Study," in *2014 IEEE 28th International Parallel and Distributed Processing Symposium*, May 2014, pp. 659–668, iSSN: 1530-2075. [Online]. Available: <https://ieeexplore.ieee.org/abstract/document/6877298>
- [32] M. Diener, S. White, L. V. Kale, M. Campbell, D. J. Bodony, and J. B. Freund, "Improving the Memory Access Locality of Hybrid Mpi Applications," in *Proceedings of the 24th European MPI Users' Group Meeting*, ser. EuroMPI '17. New York, NY, USA: Association for Computing Machinery, Sep. 2017, pp. 1–10. [Online]. Available: <https://dl.acm.org/doi/10.1145/3127024.3127038>
- [33] F. Cappello and D. Etiemble, "MPI Versus MPI+OpenMP on the IBM SP for the NAS Benchmarks," in *SC '00: Proceedings of the 2000 ACM/IEEE Conference on Supercomputing*. Nov. 2000, pp. 12–12, iSSN: 1063-9535. [Online]. Available: <https://ieeexplore.ieee.org/abstract/document/1592725>
- [34] "The Cancer Genome Atlas Program (TCGA) - NCI," May 2022, archive Location: [nciglobal,ncienterprise](https://www.cancer.gov/ccg/research/genome-sequencing/tcga). [Online]. Available: <https://www.cancer.gov/ccg/research/genome-sequencing/tcga>

Appendix: Artifact Description

Artifact Description (AD)

VI. OVERVIEW OF CONTRIBUTIONS AND ARTIFACTS

A. Paper’s Main Contributions

- C_1 We introduce Pruned Depth-First Search (P-DFS), which is a DFS/backtracking pruning method that exploits the high sparsity of tumor mutation matrices to prune infeasible h -hit gene subsets early, drastically reducing the effective combinatorial search space before Weighted Set Cover (WSC) scoring/selection.
- C_2 We integrate P-DFS with HPC-focused optimizations, including bitset-based set operations (via bitwise primitives) and a distributed, topology-aware work distribution strategy (hierarchical collectives and work stealing) designed to execute the pruned search efficiently at scale.
- C_3 We evaluate pruning effectiveness, solution/coverage behavior, and strong-scaling performance on real cancer datasets, reporting large reductions in explored combinations for 4-hits and substantial end-to-end speedups over exhaustive enumeration, including results measured at very large rank counts on Fugaku.

B. Computational Artifacts

- A_1 **Core implementation** (DOI: N/A). Code repository: <https://github.com/RitvikPrabhu/P-DFS-Multihit-WSC>

Artifact ID	Contributions Supported	Related Paper Elements
A_1	C_1	Fig. 1, Fig. 3, Fig. 5–6; Table II; Alg. 2
A_1	C_2	Fig. 4; Fig. 7–10
A_1	C_3	Fig. 3; Table III–IV

VII. ARTIFACT IDENTIFICATION

A. Computational Artifact A_1

Relation To Contributions

This artifact is a snapshot of the codebase used in the paper. It lets reviewers run the full workflow (pruned DFS candidate generation, WSC-based selection, and distributed execution) and reproduce the reported results using the provided scripts and logs. Therefore, it directly supports the pruning method (C_1), the distributed execution approach (C_2), and the empirical evaluation (C_3).

Expected Results

Running the artifact should produce the same high-level outcomes reported in the paper: it (i) generates candidate k -gene (multi-hit) combinations using P-DFS, (ii) applies the WSC-based selection stage to obtain the final set of combinations, and (iii) reports pruning and runtime summaries (e.g., candidates explored vs. pruned and wall-time breakdowns across MPI ranks). These outputs substantiate the main contributions by showing that P-DFS reduces the candidate space relative to a full-enumeration baseline and, as a result, runs faster for $k \geq 3$. Moreover, the advantage should grow with k , evidenced by a progressively larger reduction in the number of combinations evaluated.

Expected Reproduction Time (in Minutes)

The expected reproduction time for this artifact is dominated by execution. Artifact setup (configure/build) takes < 1 min and artifact analysis (parsing the emitted logs into paper-style summaries) takes < 1 min. Dataset download and preprocessing typically take 10–15 min once access has been granted (the administrative time to request/obtain access to the TCGA data is not included). Execution time varies with the dataset, the number of hits, and the amount of parallelism (node/rank count). To give context, low hit thresholds can complete quickly (e.g., 2 hits typically finishes in 1–2 min), while higher hits take longer. As a representative reference point from the paper, for the BLCA dataset at 4 hits using P-DFS, execution takes about 133 min on 192 nodes and about 20 min on 3,072 nodes. In contrast, without P-DFS (full-enumeration baseline), the BLCA run at 3,072 nodes is estimated to take over 52 hours (3,120 min).

Artifact Setup (incl. Inputs)

Hardware: We ran the experiments on Fugaku (A64FX CPUs), but the artifact is CPU-only and can run on any Linux workstation or HPC cluster. Parallel runs require an MPI environment (multiple ranks across cores/nodes). No special interconnect is required for correctness; higher-bandwidth networks simply improve scaling at large rank counts. Memory and core requirements depend on the cohort size and the number of genes retained after preprocessing.

Software: The artifact is the P-DFS-Multihit-WSC repository from <https://github.com/RitvikPrabhu/P-DFS-Multihit-WSC>. Building/running it requires CMake, a C++17 compiler, an MPI runtime, and Python 3.10+.

Datasets / Inputs: The artifact uses TCGA somatic mutation files in Mutation Annotation Format (MAF) obtained via the NCI Genomic Data Commons (GDC). Access to TCGA controlled data requires an approved data access request/proposal. This requirement applies to obtaining the MAFs (administrative approval time is external to the artifact). Once access is granted, the MAFs can be downloaded from the GDC Data Portal. The pipeline then preprocesses the MAFs into (i) a

combined, bitwise-packed mutation matrix (genes \times samples, tumor and matched-normal) and (ii) a gene map used to decode outputs. The artifact is cohort-agnostic: it can be run on any TCGA cancer type/cohort provided as input in this format.

Installation and Deployment: To install and build the artifact, clone the repository and compile the MPI executable with CMake (we recommend the Ninja backend). There are two build-time settings you choose up front:

- **Hit threshold (k):** set NUMHITS to the number of genes per combination you want to search for (e.g., NUMHITS=2 for 2-hit, NUMHITS=4 for 4-hit).
- **Mode (pruned vs. baseline):** set BOUND=ON to enable pruning (P-DFS) or BOUND=OFF to disable pruning (exhaustive enumeration baseline).

A typical configure/build sequence (pruned P-DFS) is:

```
>> git clone https://github.com/RitvikPrabhu/ \
  P-DFS-Multihit-WSC.git
>> cd P-DFS-Multihit-WSC
>> mkdir -p build && cd build
>> cmake -G Ninja .. -DNUMHITS=<k> -DBOUND=ON
>> ninja
```

To build the exhaustive baseline instead, re-run CMake with BOUND=OFF and rebuild:

```
>> cmake -G Ninja .. -DNUMHITS=<k> -DBOUND=OFF
>> ninja
```

This produces the MPI executable used in the experiments. Exact option names and example configurations are provided in the repository README.

Artifact Execution

Assuming the cohort MAF files have already been downloaded from GDC, artifact execution consists of three dependent tasks: (1) *MAF preprocessing* \rightarrow (2) *merge/pack into solver input* \rightarrow (3) *MPI run*.

- **Task 1: MAF preprocessing (downloaded MAFs \rightarrow intermediates).** Run the preprocessing script on the GDC download directory. It scans the MAFs, filters to functionally relevant mutation types, and separates tumor vs. matched-normal calls. It produces two intermediate files (written to the current working directory): a tumor mutation matrix and a normal mutation list.

```
>> python3 utils/preprocessing_maf.py \
  <GDC_COHORT_DIR>
```

- **Task 2: Create the combined solver input (intermediates \rightarrow packed input + gene map).** Convert the tumor/normal intermediates into the final solver input: a bitwise-packed combined mutation matrix (genes \times samples) and a gene-map file used to decode output indices. This step also sorts genes from most sparse to least sparse.

```
>> python3 utils/process_gene_data.py \
  <Tumor_matrix_*.txt> \
  <Normal_list_*.txt> \
  <packed_input.bin>
```

- **Task 3: MPI execution (packed input \rightarrow metrics + result tuples).** After building the executable as described in the Installation and Deployment section, launch the

solver with MPI. The run consumes the packed input from Task 2 and creates (i) a metrics file (timing/pruning summaries) and (ii) an output file containing one k -hit combination per line as a tuple of gene indices.

```
>> mpirun -np <ranks> ./run \
  <packed_input.bin> <metrics.txt> \
  <output.txt>
```

Experimental parameters. The reproduction-critical parameters are: (i) the cohort directory passed to Task 1, (ii) the hit threshold k (set at compile time via NUMHITS), (iii) pruning mode (set at compile time via BOUND: ON for pruned P-DFS, OFF for exhaustive baseline), and (iv) the parallelism level (MPI rank count in the run command). We report wall time and pruning metrics from the emitted logs. Repetitions are optional. If you want to reduce run to run timing variability you can repeat a configuration three times and report the median.

Artifact Analysis (incl. Outputs)

Each run writes the two output files that you pass as arguments to the MPI executable. The combinations file stores the selected combinations. It contains one k hit combination per line. The solution itself is the parenthesized tuple of gene indices (i_1, i_2, \dots, i_k) . The tuple length equals k . Lines may also include additional per combination fields that indicate the pruning statistics. The gene indices refer to the gene ordering produced during preprocessing rather than gene names. A gene map file is produced during preprocessing and it defines the mapping from index to gene name.

Convert indices to gene names. To translate tuples into gene names, use the conversion script with the solver output file and the gene map file produced during preprocessing.

```
>> python3 utils/convertIndexToGeneName.py \
  <output.txt> <gene_map>
```

Verify tumor coverage. To check coverage, use the verification script with the tumor and normal intermediates from preprocessing and the solver output file. The script reports whether the result file achieves the expected tumor coverage and it can list uncovered samples.

```
>> python3 utils/verifyAccuracy.py \
  <tumor_matrix.txt> <normal_list.txt> \
  <output.txt>
```

Use the output files to report the final selected combinations for each configuration. Use the timing information printed during execution or recorded in the logs to summarize wall time across node and rank counts and across hit thresholds.